JOURNAL OF AIRCRAFT
Vol. 32, No. 6, November–December 1995

Dynamic Airfoil Flow Separation and Reattachment

Lars E. Ericsson*
Mt. View, California 94040

An analysis has been performed of existing theoretical and experimental results to determine the flow physics responsible for the observed delay of flow reattachment to a negative flow incidence in a modestly rapid pitch-down motion of an airfoil. It is found that the responsible flow physics are essentially the same as those causing dynamic overshoot of static lift maximum in pitch-up motions, i.e., the accelerated flow and moving wall effects. The analysis shows that the dominant role played by the moving wall effect during pitch-down motions is in agreement with existing experimental results for a rotating circular cylinder. Applying the moving wall effect, measured through the Magnus lift on a rotating circular cylinder, to an airfoil describing pitch-down motions produces predictions that are in good agreement with experimental results. A thorough understanding of this moving wall effect is required for prediction of the high-alpha unsteady aerodynamics of advanced aircraft.

Nomenclature

b = wingspan
c = reference length, airfoil chord
c_μ = steady blowing coefficient, Ref. 26
$\langle c_\mu \rangle$ = oscillatory blowing coefficient, Ref. 26
F^+ = reduced frequency of oscillatory blowing, Fig. 16
f = oscillation frequency
K_1 = constant in Eqs. (2)
K_2 = constant in Eqs. (3)
L' = sectional lift, coefficient $c_l = L'/(\rho_\infty U_\infty^2/2)c$
l = rolling moment, coefficient $C_l = l/(\rho_\infty U_\infty^2/2)Sb$
M = freestream Mach number
N' = sectional normal force, coefficient $c_n = N'/(\rho_\infty U_\infty^2/2)c$
p = roll rate
R = radius of nose droop, Fig. 14
Re = Reynolds number, $U_\infty c/\nu_\infty$
r_N = airfoil nose radius
S = reference area, projected wing area
t = time
U = velocity
x = distance from the leading edge
z = translatory coordinate
α = angle of attack
α_0 = mean angle of attack
Δ = amplitude or increment
$\Delta\zeta$ = dimensionless z amplitude, $\Delta z/c$
ζ = dimensionless z coordinate, z/c
θ = perturbation in pitch
ν = kinematic viscosity
ξ = dimensionless x coordinate, x/c
ρ_N = dimensionless nose radius, r_N/c
ρ_∞ = air density
σ = inclination of roll axis
ϕ = roll angle
ω = angular frequency, $2\pi f$
$\bar{\omega}$ = dimensionless frequency, $\omega c/U_\infty$

Subscripts
a = accelerated flow
CG = center of gravity or rotation
d = decelerated flow
dyn = dynamic
h = hysteresis
ir = incipient reattachment
LE = leading edge
max = maximum
N = nose
r = reattachment
s = separation
W = wall
w = wake
1, 2 = numbering subscripts
∞ = freestream conditions

Derivative Symbols
$C_{l_{\hat{p}}} = \partial C_l/\partial(pb/2U_\infty)$
$c_{l_{\dot{\alpha}}} = \partial c_l/\partial\dot{\alpha}$
$\dot{\theta} = \partial\theta/\partial t$

Introduction

THE experimental results obtained by Niven and Galbraith[1] for down-ramp motion of airfoils from fully stalled conditions (Fig. 1) beg for an explanation of the underlying flow physics. A satisfactory understanding of these dynamic characteristics is critical for prediction of wing rock of aircraft with wings of moderate sweep,[2] such as the Gnat aircraft[3] or the

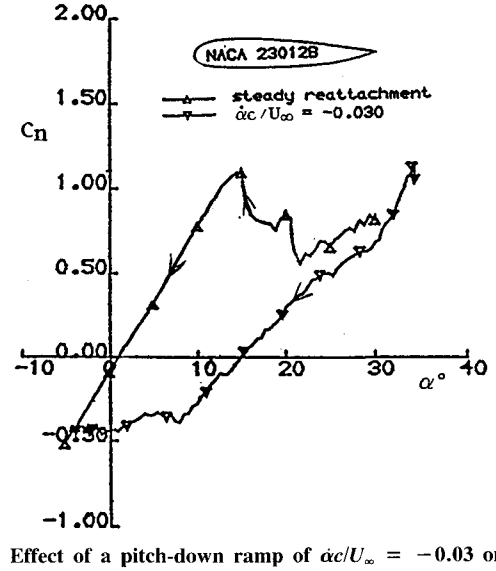

Fig. 1 Effect of a pitch-down ramp of $\dot{\alpha}c/U_\infty = -0.03$ on airfoil normal force.[1]

Received Jan. 17, 1995; revision received April 19, 1995; accepted for publication April 25, 1995.
*Engineering Consultant. Fellow AIAA.

X-29A.[4] The loss of roll damping of the X-29A aircraft[4] (Fig. 2a), initiating the wing rock (Fig. 2b), is caused by the negative damping-in-plunge generated by the airfoil sections on the rocking wing at penetration of the static stall region.[2] This loss of damping is illustrated by the two-dimensional experimental results by Liiva et al.[5] for plunging oscillations (Fig. 3). Dynamic stall concepts developed earlier[6] will be applied to determine the flow physics behind the unusual experimental results in Fig. 1. When attempting to apply two-dimensional dynamic stall results to the problem of aircraft wing rock, in addition to the three-dimensional flow effects for a constant angle of attack along the span, caused mainly by the

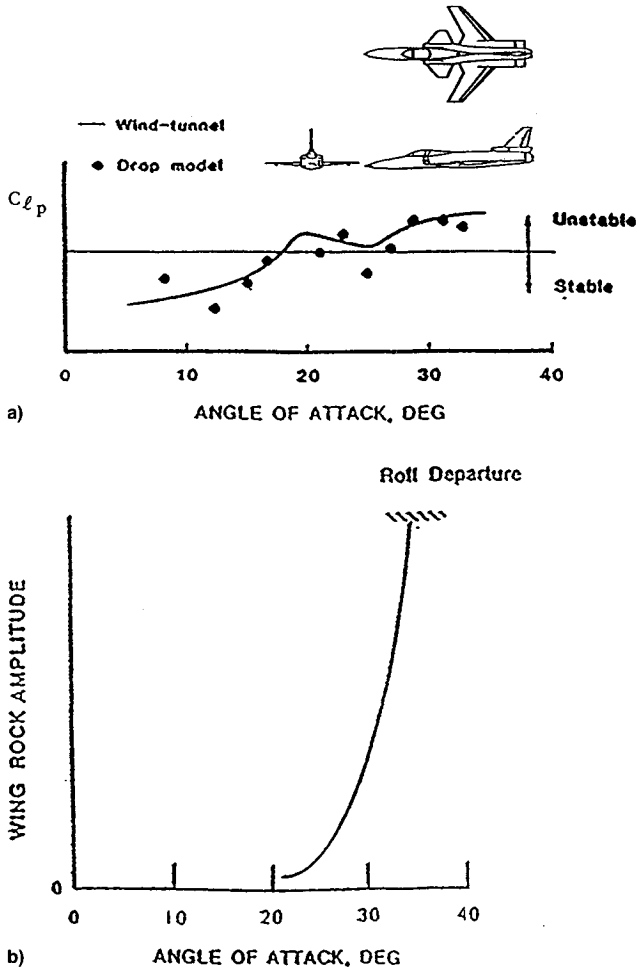

Fig. 2 Wing rock of the X-29 A aircraft[4]: a) roll damping of X-29A models and b) wing rock amplitude of the X-29A aircraft.

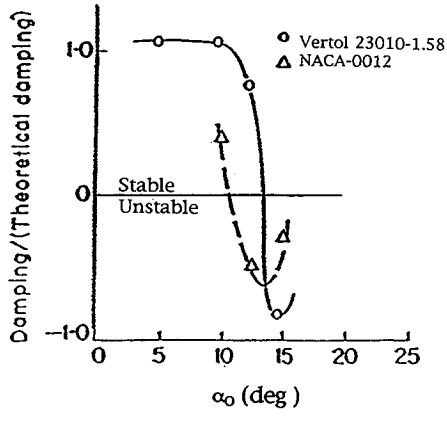

Fig. 3 Airfoil damping-in-plunge at $M = 0.4$, $\bar{\omega} = 0.136$, and $\Delta\zeta = 0.158$ (Ref. 5).

effect of a free wingtip,[7,8] one has to consider the observation made by Tarzanin.[9] His test showed that on a rotating helicopter blade dynamic stall (and reattachment) did not occur gradually along the span, dictated by the local, dynamic, crossflow angle of incidence. Instead, the switch from attached to separated flow occurred simultaneously on a large spanwise portion, extending 40% or more inboard from the tip. In that respect, the on-off flow separation and attachment is as sudden as in the case of two-dimensional flow. The different motion relationships for pitching and plunging motions will, therefore, in all likelihood not change from what has been described previously for two-dimensional flow.[6]

Analysis

The overshoot of the static stall angle α_s by an airfoil in pitch-up motion has two components,[6] $\Delta\alpha_w$ and $\Delta\alpha_s$. The component $\Delta\alpha_w$ is a pure time lag effect, generating a phase lag of the otherwise unchanged static force vector. This causes the airfoil to attain the static force after a time increment Δt at an angle of attack $\alpha(t + \Delta t)$ that exceeds the static value by $\Delta\alpha_w \approx \dot{\alpha}\Delta t$. The other component, $\Delta\alpha_s$, generates a change of the magnitude of the force vector from its static value. The resulting increase of the lift maximum by $\Delta c_{l\max} \approx c_{l\alpha}\Delta\alpha_s$ is due to the improvement of the boundary-layer characteristics through accelerated flow and moving wall effects,[6] generated by the pitch-up motion of the airfoil.

From Ref. 6 one obtains the following definition of the dynamic overshoot $\Delta\alpha_s$ of α_s:

$$\Delta\alpha_s = \Delta\alpha_{s1} + \Delta\alpha_{s2} \tag{1}$$

The component $\Delta\alpha_{s1}$ is generated by the accelerated-flow effect on the ambient pressure-gradient time history. It is only determined by the rate of change of the effective angle of attack and can be written as follows for pitching and plunging oscillations, respectively:

$$\Delta\alpha_{s1} = K_1\dot{\alpha}c/U_\infty \tag{2a}$$

$$\Delta\alpha_{s1} = K_1\dot{z}_{LE}/U_\infty \tag{2b}$$

The other component, $\Delta\alpha_{s2}$, is generated by the leading-edge jet effect (Fig. 4). In a first approximation $\Delta\alpha_{s2}$ is proportional to the plunging velocity $\dot{z}_{LE}$. For pitching and plunging oscillations $\Delta\alpha_{s2}$ becomes, respectively:

$$\Delta\alpha_{s2} = K_2\xi_{CG}\dot{\alpha}c/U_\infty \tag{3a}$$

$$\Delta\alpha_{s2} = -K_2\dot{z}_{LE}/U_\infty \tag{3b}$$

Combining Eqs. (2) and (3) defines $\Delta\alpha_s$ as follows for pitching and plunging airfoils, respectively:

$$\Delta\alpha_s = \Delta\alpha_{s1} + \Delta\alpha_{s2} = (K_1 + K_2\xi_{CG})\dot{\alpha}c/U_\infty \tag{4a}$$

$$\Delta\alpha_s = \Delta\alpha_{s1} + \Delta\alpha_{s2} = (K_1 - K_2)\dot{z}/U_\infty \tag{4b}$$

Equation (4a) shows that for a pitching airfoil the dynamic stall overshoot of the static maximum lift or normal force should increase with increasing ξ_{CG}. This is in basic agreement with experimental results[10] (Fig. 5), when considering the large data scatter, indicated by the use of dual symbols. Figure 6 shows that when plotted as a function of the reduced frequency $\bar{\omega}$, these experimental results for 6-deg amplitude oscillations of the NACA 0012 airfoil exhibit the same highly nonlinear behavior and associated large data scatter as those of Carr et al.[11] for 10-deg amplitude oscillations (Fig. 7). It is shown in Ref. 12 that the nonlinearity is in large part caused by the effect of the "spilled" leading-edge vortex. In earlier analysis of dynamic test results for the NACA 0012 airfoil[13] it was found that $K_2 \approx 2K_1$ in Eqs. (4). That is, for a pitching airfoil

$$\Delta\alpha_s \approx K_1(1 + 2\xi_{CG})\dot{\alpha}c/U_\infty \tag{5}$$

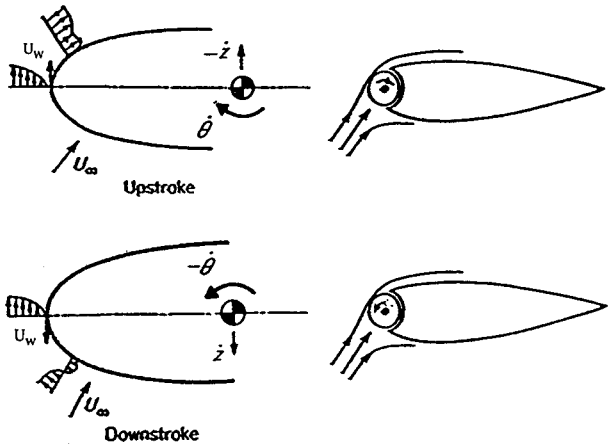

Fig. 4 Leading-edge jet effect.[6]

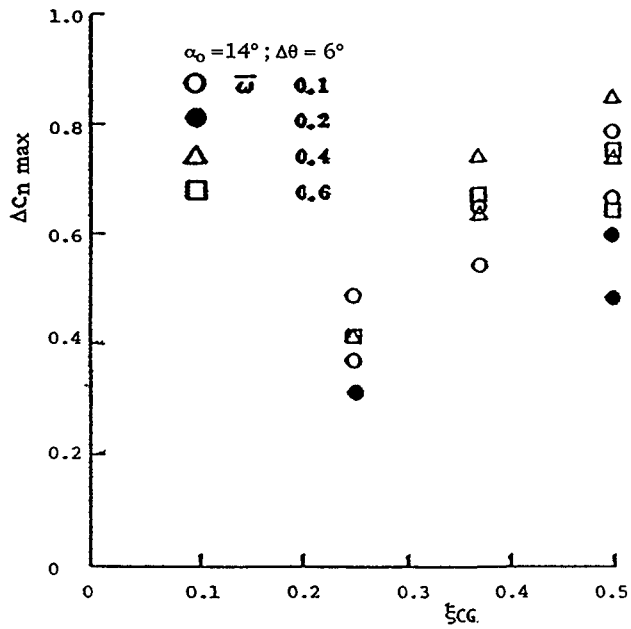

Fig. 5 Effect of rotation center location on dynamic stall overshoot of $c_{n\max}$ (Ref. 10).

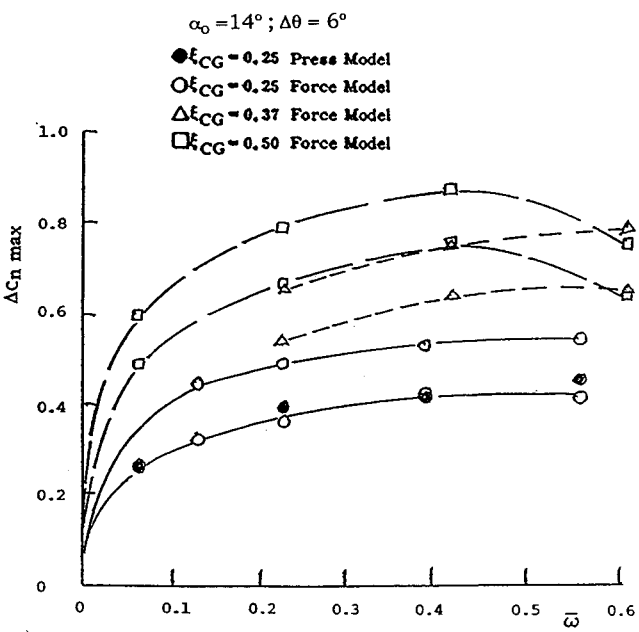

Fig. 6 Variation of $\Delta c_{n\max}$ with $\bar{\omega}$ for the NACA 0012 airfoil.[10]

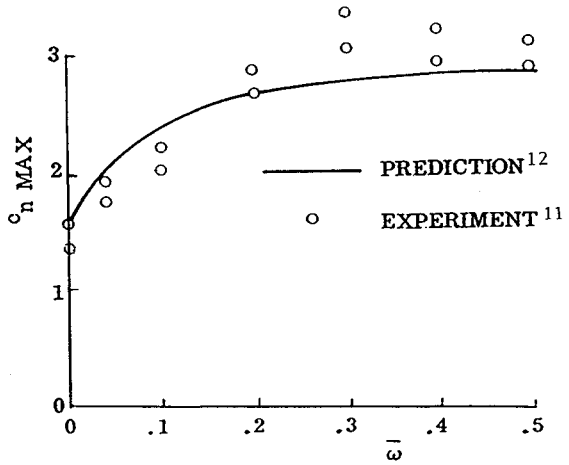

Fig. 7 Variation of $c_{n\max}$ with $\bar{\omega}$ for the NACA 0012 airfoil, ξ_{CG} = 0.25 and $\Delta\theta$ = 10 deg.

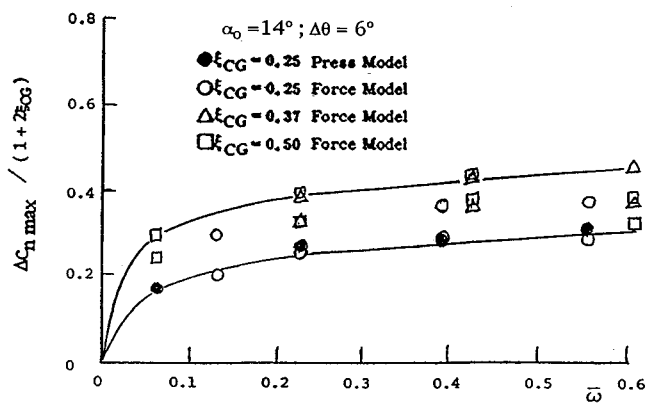

Fig. 8 Variation of $\Delta c_{n\max}/(1 + 2\xi_{CG})$ with $\bar{\omega}$ for the NACA 0012 airfoil.[10]

Figure 8 shows that when plotted in the normalized form $\Delta c_{n\max}/(1 + 2\xi_{CG})$, the experimental data from Fig. 6 tend to collapse. For $\xi_{CG} = 0.37$ and 0.50 the collapse is complete, including the envelopes of the data scatter. When considering the data scatter for each ξ_{CG} the collapse of the experimental results is satisfactory. Thus, one can represent $\Delta\alpha_s$ by Eq. (5), where $K_1 = K_u$ is the accelerated flow effect. Dynamic test results for the NACA 0012 airfoil[5] gave a value $(K_1 + K_2\xi_{CG}) \approx 3.0$ for $\xi_{CG} = 0.25$. That is, $K_1 \approx 2$ and $K_2 \approx 4$, giving $\Delta\alpha_s \approx -2\dot{z}/U_\infty$ in Eq. (4b). Thus, for a plunging airfoil the moving wall effect dominates, and promotes dynamic stall. As a consequence, plunging oscillations become undamped when stall occurs[5] (Fig. 3).

For a rolling aircraft a similar condition occurs as a result of the local plunging of the wing section, leading to a loss of roll damping and initiation of wing rock as experienced by the X-29A aircraft[4] (Figs. 2a and 2b). For the rolling wing, the effective angle of attack varies as follows with ϕ for the roll-axis-inclination σ

$$\alpha(\phi) = \tan^{-1}(\tan\sigma\cos\phi) \tag{6}$$

When $\alpha(\phi) < (\alpha_r)_{dyn}$, the plunging wing section starts generating positive damping. At the limit-cycle amplitude this includes a sufficient part of the oscillation cycle away from $\phi = 0$ to result in zero net damping. Equation (6) shows how $\alpha(\phi)$ increases with increasing inclination σ of the roll axis, requiring higher and higher roll angle ϕ to reach the condition $\alpha(\phi) < (\alpha_r)_{dyn}$. This explains the fast increase of the wing-rock amplitude with increasing angle of attack for X-29A (Fig. 2b).

Flow Reattachment

Analysis of experimental results[6,13] has indicated that also the dynamic undershoot $\Delta\alpha_r$ of static flow reattachment is proportional to the dimensionless pitch rate $\dot{\alpha}c/U_\infty$. Thus, Eq. (5) can represent $\Delta\alpha_r$ when written in the following form:

$$\Delta\alpha_r \approx -K_d(1 + 2\xi_{CG})\dot{\alpha}c/U_\infty \tag{7}$$

where K_d is the decelerated flow effect. Implicit in the formulation of Eq. (7) is the assumption that the ratio between moving wall and decelerated flow effects during the pitch-down motion is the same as that between moving wall and accelerated flow effects during the pitch-up motion. Until quantitative information becomes available for a better determination of the relative magnitudes of the two effects, this appears to be the most reasonable assumption. Its soundness is confirmed by the good agreement between prediction and experimental results, to be discussed later.

Figure 9 shows how the flow reattachment characteristics for a NACA 0015 airfoil varied with $\dot{\alpha}c/U_\infty$ in the experiment performed by Niven and Galbraith.[1] Figure 10 shows that the angles of attack for the initiation (α_{ir}) and completion (α_r) of flow reattachment, as determined from the experimental results in Fig. 9, are linearly dependent upon $\dot{\alpha}c/U_\infty$, in agreement with Eq. (7). The initial drop of α_r and α_{ir} at $\dot{\alpha}c/U_\infty = 0$ is caused by static hysteresis, as illustrated by the experimental results[14] in Fig. 11. Figure 11 also shows that the final reattachment at α_r is not always preceded by a significant incipient reattachment process.

To model the data trends in Figs. 10 and 11 one can express the flow reattachment angle of attack as follows with the aid of Eq. (7):

$$\alpha_r = \alpha_s - \Delta\alpha_h - \Delta\alpha_r \tag{8}$$

where $\Delta\alpha_r$ is given by Eq. (7), α_s is the static stall angle and $\Delta\alpha_h$ represents the delay of static flow reattachment. It remains to determine the value of K_d in Eq. (7).

A rotating circular cylinder exhibits a well-known form of moving wall effects, which is used in Fig. 4 to illustrate the leading-edge jet effect on a pitching or plunging airfoil. Figure 12 shows the Magnus lift measured by Swanson[15] on a rotating circular cylinder. In the laminar, subcritical case (Fig. 12a), the Magnus lift is generated mainly by the downstream moving wall effect on the top side, which moves the flow separation from the subcritical towards the supercritical position. On the bottom side the flow separation is occurring forward of the lateral meridian already in the static case, and the upstream moving wall effect does not have much leverage for its separation-promoting action. However, in the turbulent, supercritical case (Fig. 12b), the situation is reversed. The main effect is that of the upstream moving wall effect on the bottom side, which promotes flow separation, moving it from the supercritical towards the subcritical position. The downstream moving wall effect on the top side has very limited possibility to cause further delay of the already supercritical flow separation. Thus, the difference in Magnus lift between laminar and turbulent flow conditions is mainly the result of the difference between the capability of the moving wall effect to

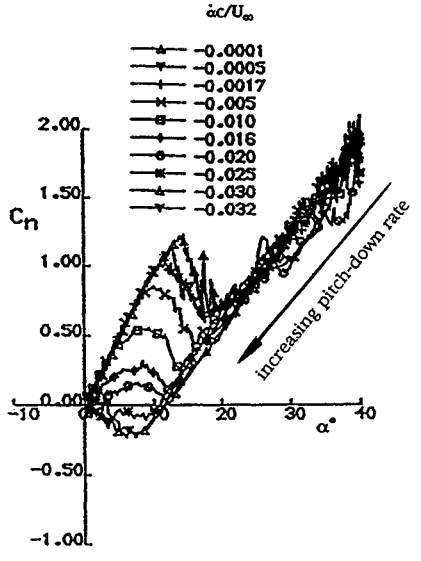

Fig. 9 Effect of dimensionless pitch rate $\dot{\alpha}c/U_\infty$ on dynamic undershoot of static flow reattachment for the NACA 0015 airfoil.[1]

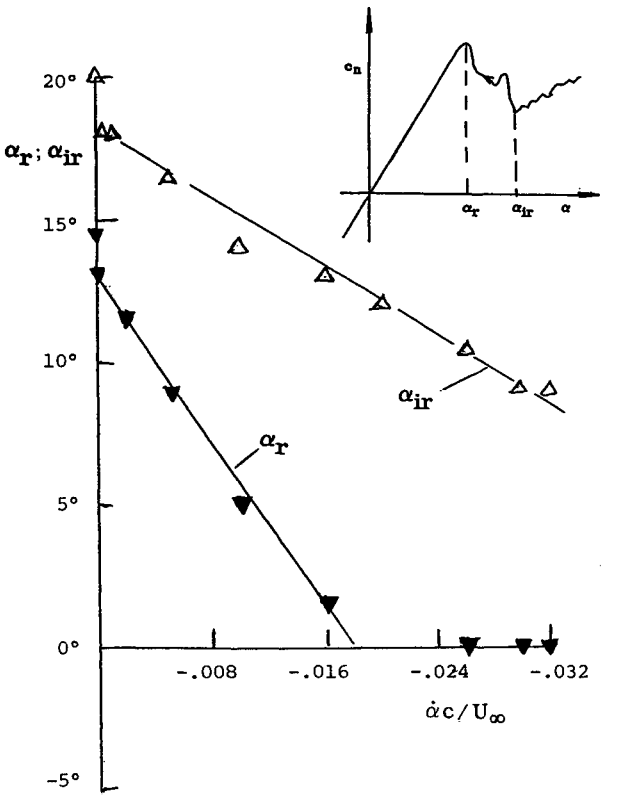

Fig. 10 Dynamic undershoot of static flow reattachment as a function of $\dot{\alpha}c/U_\infty$ for the NACA 0015 airfoil.[1]

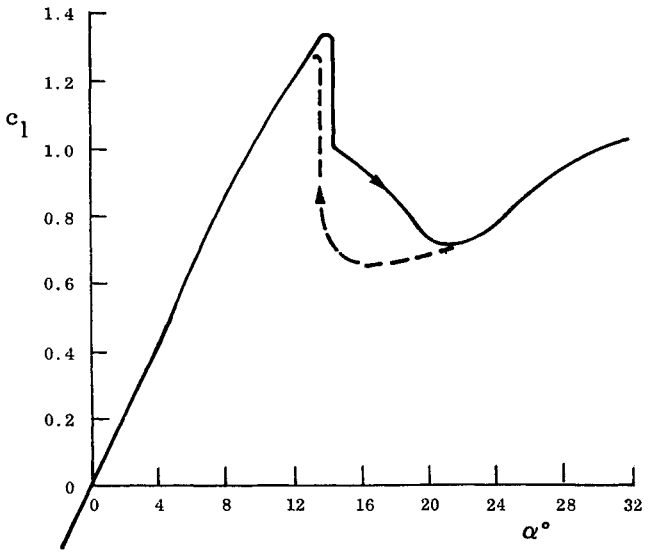

Fig. 11 Static α-hysteresis at $Re = 1.8 \times 10^6$ for the NACA 0012 airfoil.[14]

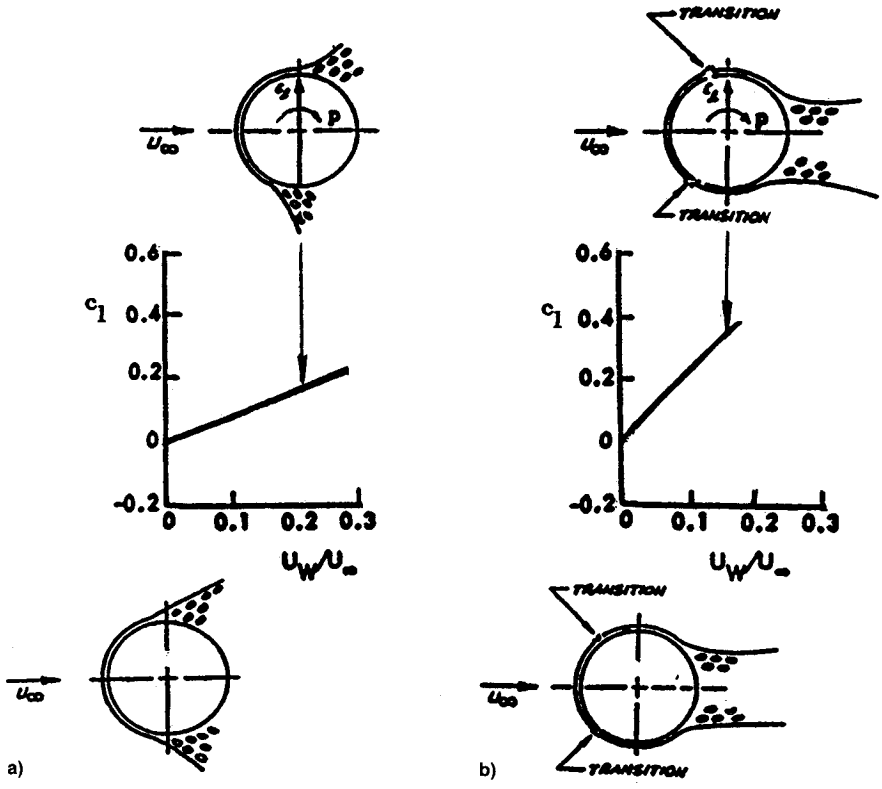

Fig. 12 Magnus lift characteristics of a circular cylinder[15]: a) laminar, subcritical flow conditions, $Re < 10^5$ and b) turbulent, supercritical flow conditions, $Re > 5 \times 10^5$.

delay laminar flow separation and promote turbulent separation. The difference in Magnus lift slopes, the laminar one being only $\frac{3}{8}$ of the turbulent one, reflects the fact that it is much more difficult to delay than to promote flow separation.

It is well established that the moving wall effect is mainly affecting the initial boundary-layer buildup close to the flow stagnation point.[16,17] Thus, it is valid to compare the moving wall effects on a rotating cylinder[15] (Fig. 12) with those on a pitching or plunging airfoil[6,13] (Fig. 4). As the moving wall effect is concentrated to the initial buildup of the laminar boundary layer near the flow stagnation point, it is very similar in Figs. 4 and 12. For lack of other applicable experimental results the 8 to 3 ratio between separation-promoting and separation-delaying moving wall effects will be used to represent also the ratio between decelerated and accelerated flow effects when comparing $\Delta\alpha_r$ to $\Delta\alpha_s$ [Eqs. (7) and (5), respectively]. Combining Eqs. (4) and (5), where $K_1 = K_a \approx 2$, with Eq. (7), where it is assumed that $K_d \approx 8K_a/3$, one obtains for $\xi_{CG} = 0.25$:

$$\Delta\alpha_r \approx -4K_a\dot{\alpha}c/U_\infty \tag{9}$$

That is, with $K_a = 2$ one obtains $\Delta\alpha_r = -8\dot{\alpha}c/U_\infty$. The experimental results in Fig. 10 give $\Delta\alpha_r \approx -13\dot{\alpha}c/U_\infty$. One would expect that K_d would be of larger magnitude for NACA 0015 than for NACA 0012 because of the difference in nose radii,[18] $\rho_N = 0.0248$ compared to $\rho_N = 0.0158$. The analysis in Ref. 18 derives the functional relationship $K_a(\rho_N)$. In the present case the analysis gives $K_a(0.0248)/K_a(0.0158) = 1.9$. As $K_a(0.0158) = 2$ for NACA 0012, one obtains for the NACA 0015 airfoil $\Delta\alpha_r \approx -15\dot{\alpha}c/U_\infty$, a value unexpectedly close to the experimental value in Fig. 10. The experimental results[1] in Fig. 13 show the expected[18] large effect of increasing nose radius. The figure also shows the large effect of camber (compare NACA 0015 with NACA 23012B). The camber increases the effective nose radius through its nose-droop effect, which has been shown to be able to increase α_s substantially[19] (Fig. 14). This explains the large effect of camber on $\Delta\alpha_r$ exhibited in Fig. 13.

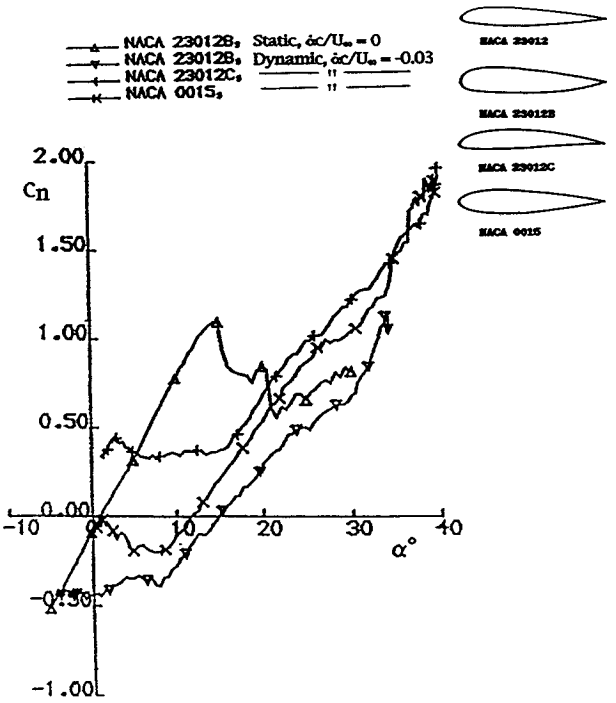

Fig. 13 Effect of nose radius and camber on dynamic flow reattachment.[1]

The described role of the moving wall effect in the flow reattachment process[20,21] is still not generally accepted. It has been suggested[22,23] that the delay of flow reattachment in Figs. 1 and 13 was caused by the "bluff body" behavior of the separated flow. Experimental results have been presented[24] for a NACA 0012 airfoil describing 10-deg amplitude oscillations at $\alpha_0 = 10$ deg and $\bar{\omega} = 0.3$, giving $|\dot{\alpha}c/U_\infty| = 0.0525$. They show that during the "downstroke motion, the bursted

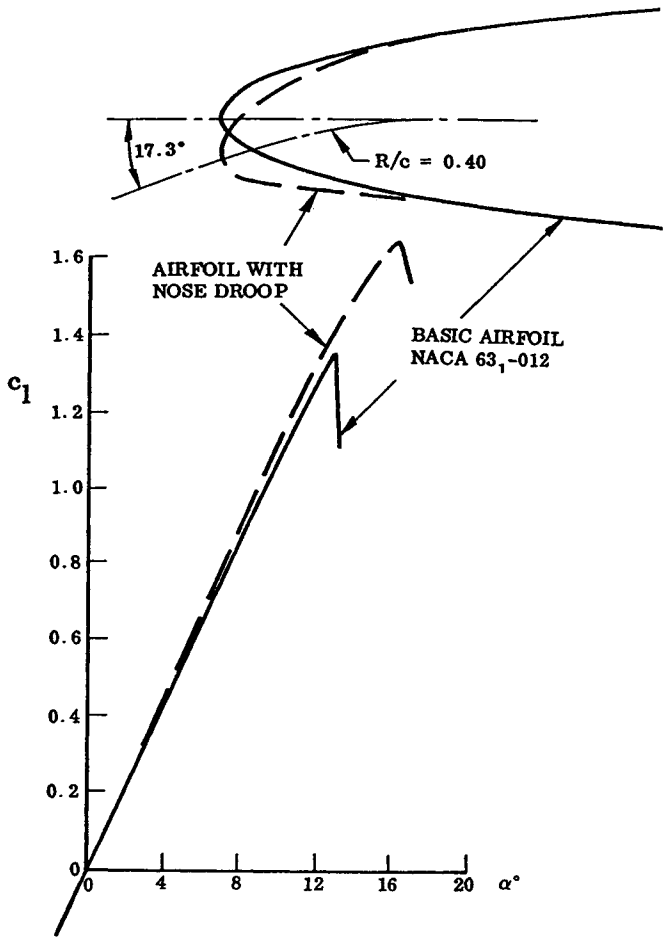

Fig. 14 Effect of nose-droop on maximum lift at $Re = 4.92 \times 10^6$ of the NACA 63_1-012 airfoil.[19]

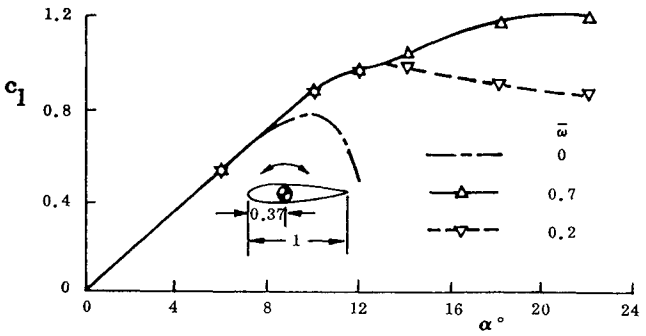

Fig. 15 Time-average lift for an airfoil describing pitch oscillations of 6.08-deg amplitude at $Re = 10^6$ (Ref. 25).

vortex disappears and then the flow reattaches uniformly beginning at the leading edge of the profile." This contrasts sharply with the "bluff body" aerodynamics described in Refs. 22 and 23, which gave rate-dependent flow reattachment at 50% chord, but rate-independent reattachment at 2.5% chord. The conclusion in Ref. 24 states that "the onset of the Dynamic Stall Vortex and the reattachment are boundary-layer driven effects," an assumption on which the moving wall effect is based.[6,12,13] The moving wall effect is, in fact, the only flow mechanism that can cause flow reattachment on an airfoil describing pitch oscillations in the deep stall region.[6,25] The data points in Fig. 15 are the time-average c_l values for 6-deg amplitude oscillations around the angle of attack $\alpha = \alpha_0$. Thus, at $\alpha_0 \approx 22$ deg the 6-deg amplitude oscillations never enter the α region below $\alpha = 16$ deg, containing the static stall condition at $\alpha \approx 10$ deg. These results necessitated the inclusion of the moving wall effect in the dynamic stall analysis in Refs. 6, 12, and 13.

When determining the magnitude of $\dot{z}_{LE}/U_\infty$, generating the moving wall effect, one is amazed by the very modest magnitude needed to produce the experimentally observed very large effects, e.g., on c_l in Fig. 15. For the 6.08-deg amplitude oscillations around $\xi_{CG} = 0.37$ one obtains $|\dot{z}_{LE}/U_\infty| \leq 0.039\bar{\omega} = 0.0078$ and 0.0274 for $\bar{\omega} = 0.2$ and $\bar{\omega} = 0.7$, respectively. Looking closer at the results in Fig. 15 one observes that only the lift values at $\alpha > 14$ deg are affected by the magnitude of $\bar{\omega}$. This influence of $\bar{\omega}$ can be related to the "spilled" leading-edge vortex, which generates a transient lift component that increases with $\bar{\omega}$, as demonstrated in Ref. 12. Thus, even lower $\bar{\omega}$ values would generate much of the measured lift increase in the deep stall region. Recently presented experimental results for a NACA 0015 airfoil[26,27] (Fig. 16), obtained using a blowing-generated "leading-edge jet," show that airfoil lift can be increased from the static $c_{l_{max}} = 0.68$

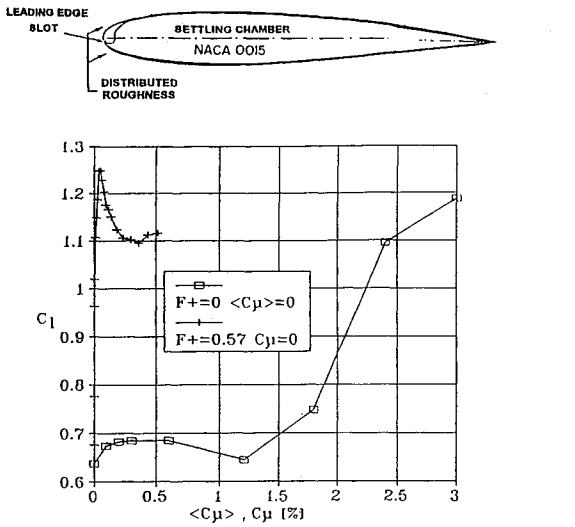

Fig. 16 Effects of leading-edge blowing on the lift of a NACA 0015 airfoil at $\alpha = 22$ deg and $Re = 0.3 \times 10^6$ (Ref. 26).

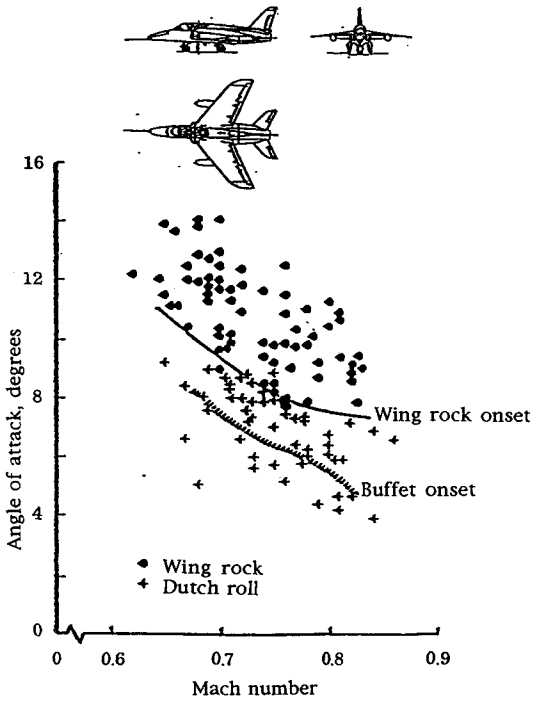

Fig. 17 Wing rock of the Gnat aircraft with tanks off.[3]

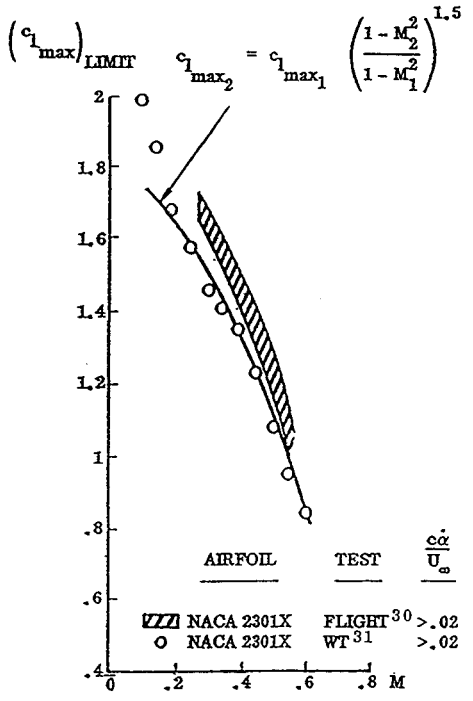

Fig. 18 Effect of compressibility on dynamic stall overshoot of maximum lift.[18]

to approximately 1.2 using steady blowing of $c_\mu = 3\%$. When using oscillatory blowing only $\langle c_\mu \rangle = 0.06\%$ was needed.

Compressibility Effects

When trying to apply results such as those in Figs. 1, 4, 6, and 10 to full-scale flight, one always has to account for the differences in Reynolds number.[28] The scaling problem is complicated greatly by the always present large effects of compressibility.[29] This is demonstrated by the wing rock results for the Gnat aircraft[3] (Fig. 17). The wing rock starts at lower and lower angles of attack for increasing subsonic Mach number because of the associated decrease in stall angle. This is in agreement with the decreasing maximum lift with increasing Mach number[18] for a pitching aircraft model[30,31] (Fig. 18). It is shown in Ref. 18 that the data trend in Fig. 18 is the result of the decrease of the effective nose radius $\rho_N = r_N/c$ with increasing Mach number due to the effect of compressibility, resulting in the predicted data trend shown by the solid line in Fig. 18.

Conclusions

An analysis has shown that the at first surprising experimental results obtained for a ramp-down motion, showing that flow reattachment can be delayed to negative angles of attack, are in good agreement with expectations based upon the existing experimental data base for dynamic airfoil stall and the Magnus lift measured on a rotating circular cylinder.

Acknowledgments

This article is in part based upon results from the initial phase of a study being performed for ARPA, Contract DAAH01-94-C-R022, under the direction of M. S. Francis.

References

[1]Niven, A. J., and Galbraith, R. A. McD., "Experiments on the Establishment of Fully Attached Airfoil Flow from the Fully Stalled Condition During Ramp-Down Motions," International Council of the Aeronautical Sciences Paper 90-3.4.3, Sept. 1990.

[2]Ericsson, L. E., "Various Sources of Wing Rock," *Journal of Aircraft*, Vol. 27, No. 6, 1990, pp. 488–494.

[3]Ross, A. J., "Lateral Stability at High Angles of Attack, Particularly Wing Rock," Paper 10, AGARD-CP-260, 1978.

[4]Fratello, D. J., Croom, M. A., Nguyen, L. T., and Domack, C. S., "Use of the Updated NASA Langley Radio-Controlled Drop Model Technique for High-Alpha Studies of X-29A Configuration," AIAA Paper 87-2559, Aug. 1987.

[5]Liiva, J., Davenport, F. J., Gray, L., and Walton, I. C., "Two-Dimensional Tests of Airfoils Oscillating Near Stall," TR 68-13, U.S. Army Aviation Labs., Fort Eustis, VA, April 1968.

[6]Ericsson, L. E., and Reding, J. P., "Fluid Mechanics of Dynamic Stall, Part I—Unsteady Flow Concepts," *Journal of Fluids and Structures*, Vol. 2, No. 1, 1988, pp. 1–33.

[7]Schreck, S. J., and Helin, H. E., "Unsteady Vortex Dynamics and Surface Pressure Topologies on a Pitching Wing," AIAA Paper 93-0435, Jan. 1993.

[8]Freymuth, P., Finaish, F., and Bank, W., "Further Visualization of Combined Wing Tip and Starting Vortex Systems," *AIAA Journal*, Vol. 25, No. 9, 1987, pp. 1153–1159.

[9]Tarzanin, F. J., Jr., "Prediction of Control Loads due to Blade Stall," AHS Preprint 513, 27th Annual Forum of the American Helicopter Society, May 1971.

[10]Windsor, R. I., "Measurements of Aerodynamic Forces on an Oscillating Airfoil," U.S. Army Aviation Labs., TR-69-98, Fort Eustis, VA, March 1970.

[11]Carr, L. W., McAlister, K. W., and McCroskey, W. J., "Analysis of the Development of Dynamic Stall Based on Oscillating Airfoil Experiments," NASA TN D-8382, Jan. 1977.

[12]Ericsson, L. E., and Reding, J. P., "Dynamic Stall at High Frequency and Large Amplitude," *Journal of Aircraft*, Vol. 17, No. 3, 1980, pp. 136–142.

[13]Ericsson, L. E., and Reding, J. P., "Dynamic Stall Analysis in Light of Recent Numerical and Experimental Results," *Journal of Aircraft*, Vol. 13, No. 4, 1976, pp. 248–255.

[14]Critzos, C. C., Heyson, H. H., and Boswinkle, R. W., Jr., "Aerodynamic Characteristics of NACA-0012 Airfoil Section at Angles of Attack from 0° to 180°," NACA TN 3361, Jan. 1955.

[15]Swanson, W. M., "The Magnus Effect: A Summary of Investigations to Date," *Journal of Basic Engineering*, Vol. 83, 1961, pp. 461–470.

[16]Dwyer, H. A., and McCroskey, W. J., "Oscillating Flow over a Cylinder at Large Reynolds Number," *Journal of Fluid Mechanics*, Vol. 61, Pt. 4, 1973, pp. 753–767.

[17]Ericsson, L. E., "Circular Cylinder Response to Karman Vortex Shedding," *Journal of Aircraft*, Vol. 25, No. 9, 1988, pp. 769–775.

[18]Ericsson, L. E., and Reding, J. P., "Stall Flutter Analysis," *Journal of Aircraft*, Vol. 10, No. 1, 1973, pp. 5–13.

[19]Kelly, J. A., "Effect of Modification to the Leading-Edge Region on the Stalling Characteristics of NACA 63_1-012 Airfoil Section," NACA TN 2228, Nov. 1950.

[20]Ericsson, L. E., "Flow Reattachment on Wings in Pitch-Down Motion," International Council of the Aeronautical Sciences Paper 94-3.4.4, Sept. 1994.

[21]Ericsson, L. E., "Pitch-Down Dynamic Stall Characteristics," AIAA Paper 94-0535, Jan. 1994.

[22]Green, R. B., and Galbraith, R. A. McD., "Phenomena Observed During Aerofoil Ramp-Down Motions from the Fully Separated State," *Aeronautical Journal*, Vol. 98, Nov. 1994, pp. 349–356.

[23]Green, R. B., Galbraith, R. A. McD., Coton, F. N., Steward, J. N., and Grant, I., "Studies of the Flow over Rapidly Pitching Two Dimensional Airfoils," 2nd ICEFM Conf., Torino, Italy, July 1994.

[24]Ranke, H., "Unsteady Separation in Two-Dimensional Turbulent Flows," International Council of the Aeronautical Sciences Paper 94-4.5.1, Sept. 1994.

[25]Halfman, R. L., Johnson, H. C., and Haley, S. M., "Evaluation of High-Angle-of-Attack Aerodynamic Derivative Data and Stall Flutter Prediction Techniques," NACA TN 2533, Nov. 1951.

[26]Wygnanski, I., "The Control of Separation by Periodic Oscillations," AIAA Paper 94-2608, June 1994.

[27]Wygnanski, I., private communication, March 21, 1995.

[28]Ericsson, L. E., "Effects of Transition on Wind Tunnel Simulation of Vehicle Dynamics," *Prog. Aerospace Sci.*, Vol. 27, 1990, pp. 121–144.

[29]Ericsson, L. E., "The Problem of Dynamic Stall Simulation Revisited," *Journal of Aircraft*, Vol. 31, No. 4, 1993, pp. 782–786.

[30]Harper, P. W., and Flanigan, R. E., "Investigation of the Variation of Maximum Lift for a Pitching Airplane Model and Comparison with Flight Results," NACA TN 1734, Oct. 1948.

[31]Harper, P. W., and Flanigan, R. E., "The Effect of Rate of Change of Angle of Attack on the Maximum Lift of a Small Model," NACA TN 2061, March 1949.